

Structure and Stability of Small Boron and Boron Oxide Clusters

Michael L. Drummond,^{*,†} Vincent Meunier,^{†,‡} and Bobby G. Sumpter^{†,‡}

Oak Ridge National Laboratory, Oak Ridge, Tennessee 37831

Received: April 3, 2007; In Final Form: May 3, 2007

To rationally design and explore a potential energy source based on the highly exothermic oxidation of boron, density functional theory (DFT) was used to characterize small boron clusters with 0–3 oxygen atoms and a total of up to ten atoms. The structures, vibrational frequencies, and stabilities were calculated for each of these clusters. A quantum molecular dynamics procedure was used to locate the global minimum for each species, which proved to be crucial given the unintuitive structure of many of the most stable isomers. Additionally, due to the plane-wave, periodic DFT code used in this study a straightforward comparison of these clusters to the bulk boron and B₂O₃ structures was possible despite the great structural and energetic differences between the two forms. Through evaluation of previous computational and experimental work, the relevant low-energy structures of all but one of the pure boron clusters can be assigned with great certainty. Nearly all of the boron oxide clusters are described here for the first time, but there are strong indications that the DFT procedure chosen is particularly well suited for the task. Insight into the trends in boron and boron oxide cluster stabilities, as well as the ultimate limits of growth for each, are also provided. The work reported herein provides crucial information towards understanding the oxidation of boron at a molecular level.

I. Introduction

Boron, like carbon, is an element capable of forming strong covalent bonds and possesses an astounding variety of chemistry not only in its elemental form, but also upon forming compounds with other elements.¹ Indeed, the ground state of solid boron, often called β -boron, is thought to possess 105 atoms in its unit cell;^{1,2} 12 and 50 atom unit cell crystal structures have also been published for other low-energy allotropes.³ This varied behavior can largely be attributed to highly directed sp² valence hybridization, electron-deficient p orbitals, and a short covalent radius. Among the large diversity of boron chemistry, many desirable or unique properties are found, and as a result boron and its compounds have been exploited in diverse fields such as ceramics, dopant technology, neutron capture therapy, and thermoelectric power conversion.⁴ Because of its low atomic weight, boron has also played a key role in applications where a large energy/weight ratio are sought, such as in the development of a hydrogen economy⁵ or as a component in high-energy fuels.^{6–8}

The unusual electronic character of boron also has ramifications for small particles of boron whose structures are quite distinct from those found in the bulk phase. This fact was established by Boustani^{9,10} whose systematic Hartree–Fock (HF) calculations of B₂–B₁₄ clusters represented a culmination of earlier research.^{11–13} These calculations revealed that small boron clusters strongly favor planar or nearly planar structures, in clear contrast to the three-dimensional (3D) icosahedral motif common in the bulk elemental allotropes. A great deal of research, using both computational and experimental techniques, has been performed to explore the structure and properties of

these small boron clusters with the eventual goal of identifying and studying the transition from nanoscale phase behavior to bulklike behavior. The majority of work has approached the nanoscale to bulk transition by starting with small clusters and building upon them, although molecular dynamics (MD) has been used to explore the behavior of a “large” 24-atom system, which was found to exhibit a 3D structure.¹⁴ Additionally, a basin-hopping method in combination with plane-wave pseudo-potential density functional theory (DFT) and the Becke–Lee–Yang–Parr (BLYP) functional has also been used to explore the planar-to-tubular structural transition for B₂₀.¹⁵ However, as the current work follows the small-to-large strategy, it is appropriate to briefly note some previous studies before presenting our results.

Most work on small boron clusters has been performed on those containing no other elements. One group of researchers has used photoelectron spectroscopy in conjunction with ab initio calculations, primarily B3LYP DFT, on both neutral and anionic small clusters, including B₃ and B₄,¹⁶ B₅,¹⁷ B₆,¹⁸ B₇,¹⁹ and B₈ and B₉.²⁰ More recently,²¹ they have examined BO[−] and BO₂[−] with the same approaches and have also compiled a review.²² A second group of researchers has performed exclusively computational work, utilizing both B3LYP- and B3PW91-based DFT, as well as second-order Møller–Plesset perturbation theory (MP2), on neutral, anionic, and cationic B₄,²³ B₅,²⁴ B₆,²⁵ and B₇ clusters,²⁶ as well as neutral B₈.²⁷ Both groups report not only calculated structural data and relative energies of the calculated isomers, but often also vibrational frequencies and zero-point energies (ZPEs). As such, these results can readily be compared to the current work to build a consensus among different computational approaches (or to identify areas of disagreement). In addition to these two series of papers, stand-alone papers reporting computational results have studied B₂–B₆,²⁸ B₂–B₈,²⁹ B₇ and B₁₀,³⁰ and B₆.³¹ Also, boron hexamers have been studied with B3LYP³² in the context of exploring

* To whom correspondence should be addressed. E-mail: drummondml@gmail.com.

[†] Computer Science and Mathematics Division.

[‡] Computer Science and Mathematics Division and Center for Nanophase Materials Sciences.

boron nitride clusters. All of these results will be considered below to help determine the structures and properties of small boron clusters. In addition to this largely computational body of work, rotational spectroscopy has been used to probe the structure of B_3^{33} and thus represents a rare, direct experimental measurement of structural information. Other experimentalists have used collision-induced dissociation, monitored by mass spectrometry, to study small, positively charged pure boron fragments.³⁴

The work in this paper focuses primarily on small boron oxide clusters, which are species that have received far less attention in the literature. Experimentally, photoelectron spectroscopy was used, along with both HF and MP2 computational methods, to probe the structure of B_2O_2 .³⁵ Another technique applied previously to pure boron clusters, mass spectrometry, was used to analyze the oxygen atom transfer products resulting from colliding both molecular oxygen³⁶ and carbon dioxide³⁷ with boron. Matrix IR spectroscopy has yielded vibrational frequencies for the smallest boron oxide clusters, such as BO, B_2O , B_2O_2 , and B_2O_3 .³⁸ These same species, as well as B_3O_3 , were computationally studied using HF and MP2 as well,³⁹ B_2O_3 was also calculated using B3LYP as part of a wider study on X_2Y_3 molecules.⁴⁰

The present study differs from those discussed above in several ways. First, this research characterizes not only pure boron clusters but also small boron oxides, B_xO_y , with $0 \leq y \leq 3$ and an upper limit of 10 atoms. Furthermore, with a few exceptions only systems where $x \geq y$ are examined. The second difference is in the basis set, which uses a description based on plane-waves paired with a pseudopotential description of the core electrons, rather than the atom-centered Gaussian basis sets used in most previous studies. While this combination is typically employed in calculations of infinitely repeating solids (and, indeed, bulk boron and bulk B_2O_3 are studied in this work using just such an approach) isolated molecules can also be calculated with plane-waves by surrounding each species with enough vacuum space to render its interaction with its periodic reflections negligible. A third key aspect of this study involves addressing the difficulty of finding global minima on 3N-6 dimensional energy hypersurfaces; namely, quantum MD was applied to a variety of initial geometries for each species, thereby creating thousands of possible structural arrangements for each B_xO_y . Low-energy structures were then subjected to standard, more accurate, geometry optimization. This procedure was recently used to successfully generate small platinum and platinum oxide structures.⁴¹ The approach taken herein is much more likely to identify a global minimum than are those used in most of the research noted above (which usually involve optimizing structures found in other small elemental clusters or high-symmetry fragments of polyhedra)^{32,42} and is comparable to the basin-hopping and simulated annealing methods used elsewhere.¹⁵

For each cluster, the geometry, stability, as measured by the cluster formation energy (FE, see below), and ground-state spin are all reported. In addition, for all low-energy structures, defined as those within 1 eV of the putative global minimum for each species, vibrational frequencies were calculated, which also allowed for ZPE-corrections to the FEs. Through the use of these calculated results, the structures of small boron clusters are analyzed for patterns, as are the boron mono-, di-, and trioxide species. Furthermore, these calculated nanostructures are compared to calculated structures of bulk boron and B_2O_3 . Complementary to this structural analysis, trends in the FEs are identified to gain insight into the transition to bulk behavior.

Finally, by comparison with both previous calculations and experimental studies greater confidence can be placed in the results reported herein. Moreover, it is possible to check hypotheses proposed by experimentalists, identify areas where these hypotheses are and are not true, and guide future studies to address areas of unresolved ambiguity. All in all, the research in this paper establishes the structures of bare and oxidized boron clusters and is therefore a crucial first step in the design of fuels based on the highly exothermic and versatile oxidation of boron.

II. Computational Methods

All calculations were performed using the periodic DFT program Vienna ab initio simulation package, version 4.6.6.^{43,44} The Kohn–Sham equations were solved using the projector-augmented wave approach^{45,46} and a plane-wave basis with a 400 eV energy cutoff. The generalized gradient approximation (GGA) exchange-correlation functional of Perdew and Wang (PW91) was utilized.⁴⁷ To ease electronic convergence, a Gaussian-smearing scheme was employed with a so-called electronic temperature ($k_B T$) of 0.01 eV; however, all final results were checked to ensure integer occupancies. Electronic convergence was defined as a consistency between successive cycles of less than 10^{-4} eV. As mentioned in the Introduction, to simulate isolated molecules using a periodic code each species was placed in a cube measuring 18 Å per side, which ensured at least 10 Å of vacuum in each Cartesian direction between a molecule and its reflection. Additionally, k -point sampling was restricted to a single point, the Γ point. (For the calculation of bulk boron and B_2O_3 , which are periodic, the Brillouin zone was sampled with a $4 \times 4 \times 4$ mesh and a Monkhorst–Pack⁴⁸ scheme.) To avoid wrap-around error, reciprocal space integration utilized a $120 \times 120 \times 120$ fast Fourier transform (FFT) grid. For geometry optimizations, a conjugate gradient algorithm⁴⁹ was initially applied, which was switched to a quasi-Newton approach⁵⁰ in cases where the former method failed. Structures were considered to be converged when the forces acting upon any atom were less than 0.01 eV/Å. Symmetry constraints were not employed. All other options were left at their default values.

Determining the global minimum for any structure with more than four atoms is often a daunting task. If one simply begins optimization at intuitive structures, it is entirely possible to fail to locate a nonintuitive, lower energy structure, even if multiple, perfectly legitimate initial geometries are considered. Therefore, quantum MD was applied, which generates structures on a solely energetic basis. The starting point for any MD run is unavoidably subject to user bias, and thus multiple trajectories, (generally 8–12) were run for each B_xO_y species. The kinetic energy cutoff in these MD runs was reduced to 150 eV, as the goal was to generate a wealth of varied structures in a timely fashion, not to accurately measure thermodynamic behavior. A microcanonical ensemble was simulated with acceleration provided from the calculated Hellmann–Feynman forces and the total free energy was kept constant. The initial temperature was set to 500 K, and a time step of 0.8 fs was chosen. Each trajectory was run for a maximum of 3000 time steps, although runs were sometimes halted because of failed electronic convergence or dissociation of the cluster; the redundancy of multiple trajectories helped to ensure that no relevant information was missed because of these premature terminations. Especially for some of the structures with a lower boron-to-oxygen ratio, this MD procedure often led to quick dissociation of the cluster. In such cases, a Nosé–Hoover MD approach⁵¹ with a thermostat of 0.1 and an initial temperature of 500 K

was used, which proved far less likely to cause dissociation. Indeed with this methodology, starting geometries often quickly rearranged to a lower energy structure and then did not change significantly for hundreds of time steps.

Regardless of the specific MD approach used, a number of low-energy structures were chosen and subsequently subjected to the more accurate geometry optimization described above. Note that not only were the lowest energy structures chosen for each trajectory, as this choice tended to provide fairly similar structures, but low-energy local minima generated by the MD procedure were also optimized to increase the variety of structures optimized. For pure boron clusters, trajectories were run on both low-spin (i.e., singlet for even-numbered clusters and doublet for odd-numbered clusters) and high-spin (similarly, triplet and quartet, respectively) surfaces. However, the data generated by the high-spin runs did not prove to be very informative, as low-energy triplet and quartet structures could always be generated by optimizing their low-spin geometries in a high-spin configuration. Thus, for all boron oxides MD was performed only on the lowest spin surface, and all optimized low-spin structures were also optimized in their high-spin configurations. All higher spin-state (doublet, triplet, and quartet) structures given in this paper were carefully checked for spin contamination by evaluating $\langle S^2 \rangle$ using NWChem with the PW91 functional and a 6-311G** basis set;⁵² no significant contamination was found.

For the lowest energy structure for each species and for each structure within 1 eV of this global minimum, vibrational frequencies were also calculated. Each atom was displaced in both positive and negative directions by 0.01 Å along all three Cartesian axes. The forces calculated from these distorted structures were then used to generate the Hessian matrix, the diagonalization of which yields the normal modes and associated vibrational frequencies. This method also generates three translational and three rotational frequencies, which tend to be low energy and can be either real or imaginary. Thus, the six frequencies with the lowest eigenvalues, both real and imaginary, were treated as the translations and rotations and thus were disregarded. Structures with imaginary frequencies were optimized further at tighter convergence criteria (using the `prec = accurate` setting) and had their frequencies recalculated at these strict standards to prevent the mislabeling of numerical inaccuracies as imaginary frequencies. The ZPE was calculated as one-half the sum of the (real) calculated vibrational frequencies multiplied by Planck's constant.⁴¹ The ZPE correction is less than 0.05 eV per atom for all clusters in this work.

III. Results

Bulk Structures. The calculation of bulk structures, which possess a number of experimentally well-known parameters, not only provides a gauge of the accuracy of the cluster calculations, but also serves as the ultimate end-point of cluster formation. For elemental boron, the 105-atom rhombohedral arrangement, β -boron, was calculated. The initial atomic positions and lattice constants of Geist et al.² were used. This allotrope of boron belongs to space group 166, $R\bar{3}m$, with a rhombohedral lattice constant of 10.17 Å and an accompanying angle α of 65.20°; the calculated values are 10.12 Å and 65.25°, respectively, in good agreement. Because of the complexity of the structure, we omit further description and simply note that the calculated coordinates are in very good agreement with experiment and point toward ref 3 for a full, elegant visual depiction.

B₂O₃ does not crystallize in nature; a glassy polymorph instead forms. Although MD studies have attempted to repro-

duce the characteristics of this vitreous phase,^{53,54} the discussion here is limited to the crystalline form generated under special conditions.⁵⁵ The polymorph stable at ambient pressure was calculated in this work.⁵⁶ This crystal belongs to space group 152, $P3_121$, with experimental lattice constants of $a = 4.3358$ Å and $c = 8.3397$ Å. The calculated values are 4.2996 and 7.9980 Å, respectively. Although the agreement for these lattice constants is poorer for B₂O₃ than it was for β -boron, the average calculated B–O distances of 1.367 and 1.375 Å are in good agreement with the experimental values of 1.356 and 1.374 Å, respectively.

From the optimized geometries of these two crystals, bulk moduli were calculated. The calculated value for β -boron, 194 GPa, compares well to the experimental value of 185 GPa.⁵⁷ To the best of our knowledge, no experimental measurement of the bulk modulus of crystalline B₂O₃ exists, although previous DFT calculations have set it at 26 GPa,⁵⁸ using a local density approximation, and 60 GPa,⁵⁹ using the same PW91 functional employed in this work. Although the presently calculated value of 88 GPa is, unsurprisingly, more in line with the latter of these values, the accord is quite poor. While some of the discrepancy is certainly because of the use of different codes and while bulk moduli are notoriously difficult to calculate accurately,⁶⁰ this disagreement may indicate that special care should be taken in optimizing B₂O₃.

The stability of the bulk structures was also determined, through measurement of the formation energy (FE). For bulk solids and isolated clusters alike, this quantity defined as $E_{B_xO_y} = \sum / E_{\text{products}} - \sum / E_{\text{reactants}}$ on a per boron basis, was chosen so meaningful comparisons could be made between the bulk and the cluster structures, as well as between pure boron and boron oxide clusters. A negative FE for a species indicates that it is stable with respect to its components. The FE of a pure boron cluster is, therefore, the negative of the cohesive energy commonly reported in solid-state calculations; the cohesive energy multiplied by the number of atoms in a cluster is therefore the atomization energy. Furthermore, the FE of a bulk compound is simply the heat of formation given on a per boron basis. The calculated FE of -6.37 eV/B for bulk β -boron is in fair agreement with an experimental value of -5.81 eV/B.⁶¹ Similarly, the FE of bulk B₂O₃ was found to be -6.14 eV/B, somewhat off from the tabulated value⁶² of -6.59 eV/B. Additionally, the FE of boron dimer has been experimentally measured; its value of -1.50 eV/B⁶³ is again somewhat missed by the calculation, which gives a value of -1.83 eV/B. Thus, it seems that an accuracy of a few tenths of an eV per boron can be expected, thereby yielding acceptable trends, if not quantitative accuracy. This is especially true considering that errors should be systematic among the family of B_xO_y clusters.

Pure B Clusters. The lowest energy boron clusters are shown in Figure 1. Bond distances, except for certain values mentioned in the text, are provided as Supporting Information. Accompanying relative stabilities (as measured by zero-point corrected formation energies), lowest energy spin state, and vibrational frequencies are listed in Table 1. Note that for both B₄ and B₆, two structures are pictured and tabulated; these species each possessed a second isomer with a total energy within 0.2 eV of the proposed global minimum.

A few comments can be made about these structures. Most obviously, as suggested and developed elsewhere,^{9,10,64} these bare boron clusters have a strong tendency toward planarity. Indeed, B₂–B₅, B₆-g (that is, the isomer shown in Figure 1g), and B₈ are all planar to within a few hundredths of an angstrom. Even for the remaining structures, most of the atoms are

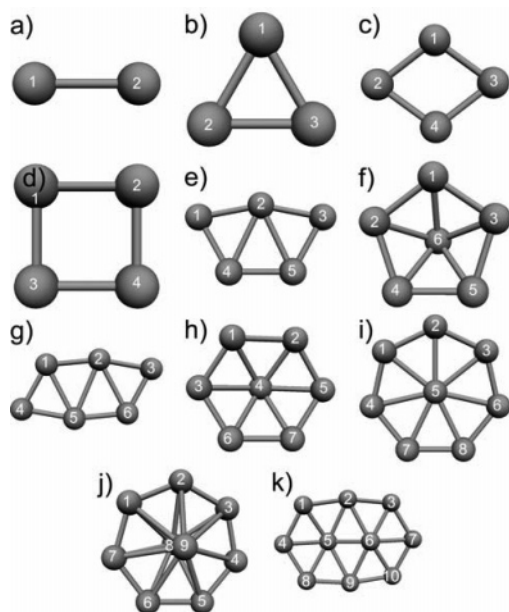


Figure 1. Calculated lowest energy structures of (a) B_2 , (b) B_3 , (c) and (d) B_4 , (e) B_5 , (f) and (g) B_6 , (h) B_7 , (i) B_8 , (j) B_9 , and (k) B_{10} . The atom numbers refer to the bond distances given as Supporting Information.

coplanar with exceptions being atom no. 6 of B_6 -f, no. 4 of B_7 , nos. 8 and 9 of B_9 , and nos. 5 and 6 of B_{10} . Interestingly, these atoms are all center atoms of larger boron rings, although the coplanarity of no. 5 of B_8 proves that not all central atoms are found out-of-plane.

Turning to Table 1, it appears that despite the near indistinguishable formation energies of the two isomers of B_4 , -4.00 and -3.98 eV/B for Figure 1, structures f and g, respectively, vibrational analysis identifies only B_4 -f as a genuine minimum with B_4 -g being a transition state connecting the B_4 -f isomer shown with one rotated by 90° . The calculated frequencies in and of themselves do not distinguish the two isomers of B_6 , however. Additional considerations, both of an experimental and computational nature, will be discussed later to allow an assignment of the most likely true minimum. Finally, with the exception of B_9 , the FE of each cluster increases with cluster size. B_9 , it would appear, is too small to form an oblong ring, as B_{10} does, but an atom-centered octagonal ring is apparently also unfavorable, according to the calculations. Thus, the two central boron atoms orient themselves perpendicular to the larger ring, which is an arrangement not found in any other B_xO_y cluster explored in this work, likely reflecting its unfavorable energy, which in turn causes a slight downturn in the FE trend.

B_xO Clusters. The structures and relevant data for the boron monoxide clusters are given in Figure 2 and Table 2. As was the case with the pure boron clusters, the B_xO clusters have a strong tendency toward planarity. The two exceptions to this trend are B_7O , which is clearly built from the similarly nonplanar B_7 , and B_9O -n, which is identified by vibrational analysis as a second-order saddle point and therefore probably not relevant. In every case except B_2O , oxygen adds to the exterior of a central boron cluster. To make an analogy with carbonyl chemistry, oxygen can occupy either a terminal or a bridging position. When the former motif is present, the B–O bond distance is the same as in isolated BO, $1.215 \text{ \AA} \pm 0.001 \text{ \AA}$. The sole exception is in B_4O -e, where the B–O bond distance is 1.245 \AA . Moreover, the distinction between terminal and bridging oxygen, as well as that between B_4O -e and all other

terminally bound oxygen atoms, is readily apparent in the vibrational frequencies. In particular, all terminal B–O-stretching frequencies are found between 1900 and 2000 cm^{-1} with the exception of B_4O -e with a stretching frequency of 1682 cm^{-1} . In further analogy to carbonyl-stretching frequencies, bridging oxygens stretch at lower energies, roughly 1300 – 1600 cm^{-1} . However, the vibrational delineation between terminal and bridging regimes seems to be more flexible in boron oxides than in carbonyl compounds, as the bridging O in B_9O -m is calculated to stretch at 1700 cm^{-1} , which is higher in energy than the stretching frequency of B_4O -e. Nevertheless, if this caveat is kept in mind, it appears that vibrational spectroscopy may prove quite useful in giving structural clues about boron oxide clusters.

In general terms, it seems that the structures of the monoxides can be rationalized as a balance between three patterns. The first pattern is a linear arrangement of atoms (or nearly so, as the B–O–B angle in B_2O is 175°). This tendency, which was not operative for even a three-atom cluster in bare boron, provides the lowest energy structure for all monoxides up to and including the five-atom B_4O . At B_4O , however, two other patterns are also found. The second pattern in B_xO structure is simply the addition of a bridging oxygen atom to the lowest energy B_x structure. This rationalization successfully predicts the lowest energy structures of B_5O , B_7O , and B_8O . The third possibility is to consider B_xO as consisting of a BO moiety, noted above as highly conserved throughout various isomers, combined with a low-energy structure of B_{x-1} . While, as noted above, B_4O -e may be an atypical example, it can be thought of as $B_3 + BO$; B_5O -h and B_6O are also examples. It is even possible to rationalize the lowest energy, linear structures of B_3O and B_4O as simply $B_{x-1} + BO$. In fact, the lowest energy isomer of B_9O is built from BO plus a B_8 structure not even identified as a low-energy structure by the MD procedure, perhaps indicating that a B–O fragment extended from a core cluster is an especially favorable way to incorporate oxygen into a boron cluster. These rationalizations of oxygen placement will be further developed in the context of the dioxides and trioxides.

B_xO_2 Clusters. Figure 3 and Table 3 describe the structures and properties of the small boron dioxide clusters. Without exception, the oxygen atoms do not embed themselves in the clusters but prefer to be located on the outside of the larger boron framework. Also, immediately noticeable is the strong tendency for the two oxygen atoms to avoid each other with the sole exception being B_7O_2 . This species is also the only cluster that deviates from planarity (boron no. 5 is out-of-plane, as are both oxygen atoms); it is unclear if the two facts are related. Clearly, many of the structures from Figures 1 and 2 are preserved as a second oxygen atom is introduced, for example, B_6O_2 (Figure 3f) can be considered as Figure 2i with an additional bridging oxygen, or as Figure 1e with both a bridging oxygen and a B–O moiety added. The connection between B_7 , B_7O , and B_7O_2 , as well as between B_8 , B_8O , and B_8O_2 , is readily apparent as well. Indeed, the three types of clusters identified above for the monoxide species, that is, linear, with a bridging O, or with a terminal BO moiety, are all present for the dioxides as well with the addition that both of the latter two motifs can be found in a single given cluster, for example, for both B_5O_2 isomers and for B_6O_2 . The larger clusters of B_7O_2 and B_8O_2 , however, possess exclusively bridging oxygen atoms. Thus, it may be that oxygen prefers to occupy a bridging site, provided that the boron ring is large enough to accommodate multiple sites; if not, then it is necessary to shift to a B_{x-1} core

TABLE 1: Calculated Formation Energies, Lowest Spin State, and Vibrational Frequencies of the Pure Boron Clusters

cluster ^a	FE (eV/B)	spin ^b	vibrational frequencies (cm ⁻¹) ^c
B ₂	-1.83	T	1012
B ₃	-3.29	D	1234, 972, 963
B ₄ -c	-4.00	S	1270, 1238, 1167, 1012, 401, 333
B ₄ -d	-3.98	S	1287, 1193, 1189, 1188, 293, 274i
B ₅	-4.21	D	1314, 1201, 1050, 951, 747, 604, 448, 324, 198
B ₆ -f	-4.45	S	1107, 1105, 1083, 1077, 1038, 808, 804, 651, 584, 583, 312, 311
B ₆ -g	-4.44	T	1366, 1310, 1116, 1075, 808, 643, 524, 502, 376, 311, 305, 207
B ₇	-4.71	D	1228, 1154, 1114, 1066, 1052, 922, 791, 759, 631, 597, 593, 444, 422, 318, 232
B ₈	-4.98	T	1394, 1393, 1243, 1240, 946, 945, 815, 716, 714, 584, 583, 479, 478, 406, 405, 282, 266, 265
B ₉	-4.96	D	1498, 1497, 1329, 1326, 974, 971, 941, 814, 461, 460, 445, 444, 376, 373, 344, 340, 339, 266, 256, 138, 137
B ₁₀	-5.17	S	1266, 1245, 1192, 1171, 1110, 1084, 1025, 1006, 862, 789, 781, 728, 701, 620, 558, 538, 500, 499, 447, 418, 410, 336, 266, 85

^a When a letter follows a cluster, refer to Figure 1 for the identity of each isomer. ^bS = singlet, D = doublet, T = triplet. ^c Imaginary frequencies are italicized.

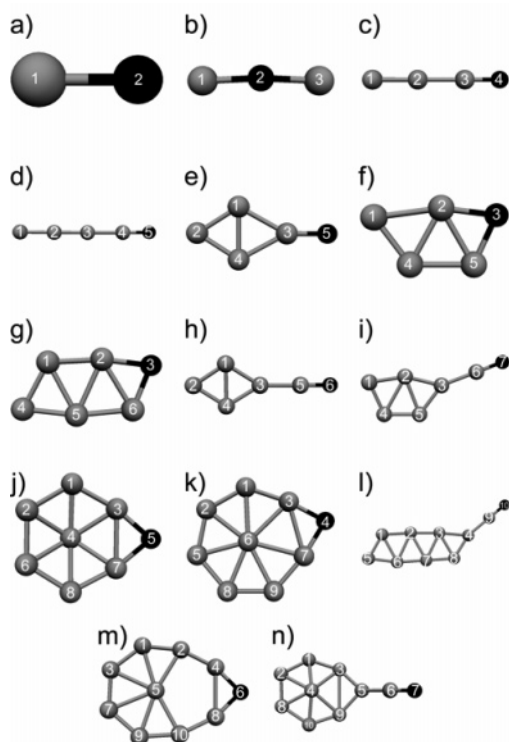


Figure 2. Calculated lowest energy structures of (a) BO, (b) B₂O, (c) B₃O, (d), (e), and (f) B₄O, (g) and (h) B₅O, (i) B₆O, (j) B₇O, (k) B₈O, (l–n) B₉O. Gray spheres are boron, black spheres are oxygen. The atom numbers refer to the bond distances given as Supporting Information.

with widely separated B–O moieties extending outward to provide the necessary oxygen separation. The amount of distance required between oxygen atoms is quite vague at this point, especially given the close proximity of the two oxygen atoms in B₇O₂. While analysis of the trioxides will help to clarify the issue somewhat, further work on larger clusters, on the order of B₁₂O₃ or B₁₄O₄, will clearly provide additional information.

A point of final interest in the dioxides concerns the vibrational characteristics of the bridging and B–O oxygen atoms. A priori, it might be expected that the introduction of a second oxygen atom would cloud the picture because of coupled B–O vibrations and inductive effects. Indeed, it does seem that the rigidity of the terminal B–O fragment is disrupted by the addition of a second oxygen atom with the B–O bond length ranging from 1.207 Å in B₂O₂ to 1.247 Å in B₅O₂-e (cf. the value of 1.215 ± 0.001 Å for almost all of the boron monoxide clusters). However, whereas for the monoxide species, vibrational analysis was imperfect in discriminating between bridging

and terminal oxygen vibrations, for the dioxides all terminal oxygen stretches are above 1724 cm⁻¹ and all but one (for B₅O₂-e) are above 1900 cm⁻¹. The bridging frequencies span a greater range, from 1373 to 1632 cm⁻¹, but are all still lower than the terminal vibrations. With the caveat of extrapolating from limited data sets, it may perhaps be most useful to extend the analogy made to carbonyl vibrational frequencies and to envision instead three regimes of B–O vibrations (see Figure 4): (a) those where the boron of the B–O moiety is attached to the greater cluster in an end-on, η¹ fashion with vibrations found above 1900 cm⁻¹; (b) those where the B–O fragment is attached to the cluster in a bridging, η² fashion with the two examples thus far, B₄O-e and B₅O₂-e, having calculated frequencies of 1682 and 1724 cm⁻¹, respectively; and (c) those where O itself attaches to the cluster in a bridging, η² fashion with a range thus far of 1700 cm⁻¹ for B₉O-m to 1315 cm⁻¹ for B₄O-f. As will be seen, additional insight into this possible trichotomy will be gathered as the trioxides are considered.

B_xO₃ Clusters. As with the other B_xO_y clusters, Figure 5 and Table 4 describe the boron trioxides. Many of the trends identified for the less-oxidized clusters are also found in these species: every structure in Figure 5 is planar, and all but the smallest two (B₂O₃ and B₃O₃-b) do not have an oxygen atom incorporated into the midst of the boron framework. The tendency for oxygen atoms to distance themselves from one another, noted for the dioxides, is also clearly operative as well for the trioxides. Additionally, just as in the B_xO and B_xO₂ clusters, oxygen can bind to boron atoms in an η¹ or in an η² fashion. However, unlike the larger B_xO₂ clusters, no trioxide species calculated contain exclusively bridging oxygens. This difference is likely a reflection of the fact that the largest trioxide calculated contains seven boron atoms, which favors a hexagonal ring (see Figure 1h). Thus, the example of B₇O₂ (Figure 3g) notwithstanding, a large ring is apparently needed to accommodate three bridging oxygen atoms. If this is true, there should be an experimental signature, observable for example using IR, of a transition from the dominance of terminal oxygen-binding motifs, as seen for trioxides up to at least B₇O₃, to the dominance of bridging oxygen-binding motifs, as seen for B₇O₂ and B₈O₂ and possibly for other larger, higher-order oxides as well. Another possibility to consider is that a nonring structure may be able to support an exclusively bridging oxygen atom arrangement, such as the “zigzag” pattern seen in, for example, B₉O-l or B₆O₃-j. In any event, more research, likely first using computational approaches but later confirmed experimentally, is needed to further explore the balance between bridging and terminal oxygen placement in boron oxides.

The vibrational information in Table 4 also supports the earlier hypothesis that different oxygen-binding motifs can be

TABLE 2: Calculated Formation Energies, Lowest Spin State, and Vibrational Frequencies of the Boron Monoxides

cluster ^a	FE (eV/B)	spin ^b	vibrational frequencies (cm ⁻¹) ^c
B ₁ O	-5.42	D	1869
B ₂ O	-3.35	S	1480, 1053, 111
B ₃ O	-1.71	Q	1955, 1368, 622, 443, 418, 185
B ₄ O-d	-0.87	T	1933, 1548, 1037, 504, 468, 442, 249, 203, 102
B ₄ O-e	-0.86	T	1682, 1241, 908, 885, 563, 393, 321, 276, 115
B ₄ O-f	-0.85	T	1315, 1219, 984, 818, 729, 599, 427, 413, 133
B ₅ O-g	-0.96	D	1451, 1210, 1201, 1020, 875, 767, 641, 567, 494, 489, 327, 210
B ₅ O-h	-0.93	D	1982, 1305, 1187, 1031, 733, 674, 492, 452, 430, 296, 128, 93
B ₆ O	-0.91	S	1968, 1384, 1274, 1121, 1040, 740, 701, 507, 451, 430, 343, 321, 267, 119, 89
B ₇ O	-0.69	S	1425, 1231, 1197, 1131, 1091, 951, 848, 816, 702, 622, 620, 557, 530, 498, 433, 372, 363, 222
B ₈ O	-0.57	S	1595, 1504, 1326, 1264, 1120, 970, 794, 789, 738, 602, 596, 570, 530, 500, 437, 418, 364, 343, 318, 242, 167
B ₉ O-l	-0.44	D	1946, 1380, 1337, 1292, 1192, 1109, 935, 798, 706, 656, 617, 561, 542, 491, 458, 452, 423, 364, 307, 273, 199, 167, 81, 61
B ₉ O-m	-0.44	D	1700, 1542, 1500, 1281, 1276, 1049, 918, 694, 676, 580, 535, 486, 462, 416, 414, 397, 363, 356, 330, 310, 224, 181, 132, 129
B ₉ O-n	-0.42	D	1915, 1333, 1313, 1198, 1073, 1001, 894, 870, 731, 676, 604, 565, 534, 478, 462, 448, 428, 405, 375, 276, 180, 123, 428i, 115i

^a When a letter follows a cluster, refer to Figure 2 for the identity of each isomer. ^bS = singlet, D = doublet, T = triplet, Q = quartet. ^cImaginary frequencies are italicized.

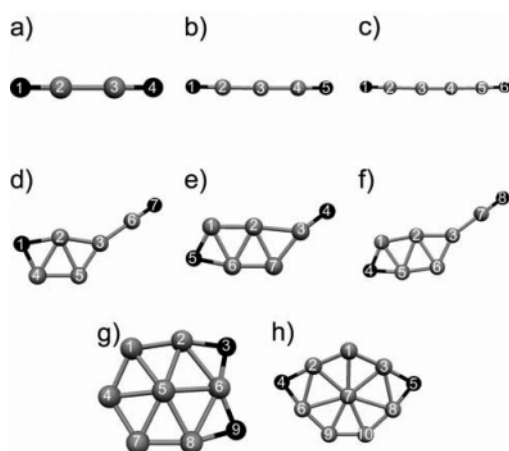


Figure 3. Calculated lowest energy structures of (a) B₂O₂, (b) B₃O₂, (c) B₄O₂, (d) and (e) B₅O₂, (f) B₆O₂, (g) B₇O₂, and (h) B₈O₂. Gray spheres are boron, black spheres are oxygen. The atom numbers refer to the bond distances given as Supporting Information.

identified via IR or Raman spectroscopy. To restate, a B–O moiety attached to another boron in an η^1 fashion (Figure 4a) stretches at higher energy than does a B–O moiety bridging between more than one boron (Figure 4b); an oxygen attached directly to more than one boron (Figure 4c) is the easiest to stretch. On the basis of all of the oxide-stretching frequencies calculated in this work, the first category ranges from 2113 (B₂O₃) to 1899 cm⁻¹ (B₂O₂). There is then a gap of 29 cm⁻¹ between the first and second regimes with the calculated oxygen-stretching frequency of B₇O₃-m found at 1870 cm⁻¹, signaling the beginning of the second area. There is a small amount of overlap between the second regime and the bridging regime, as the η^2 B–O stretch of B₃O₃-c (atoms nos. 1 and 2) is found at 1549 cm⁻¹, whereas the μ -O stretch of B₉O-m is calculated at 1700 cm⁻¹. However, both of these structures are fairly atypical, and lower-energy isomers exist for both of these species, so they may not be experimentally relevant at all. If these two stretches are ignored as exceptions, then a gap of 50 cm⁻¹ between the η^2 B–O-stretching regime and the μ -O regime is calculated, between B₄O-e (1682 cm⁻¹) and B₈O₂ (1632 cm⁻¹). The lowest energy μ -O stretch was calculated at 1315 cm⁻¹ for B₄O-f. Even if the rigidity of these delineations breaks down with increasing oxidation, in situ IR spectroscopy should be a fairly sensitive structural probe. Furthermore, consider B₇O₃-k and B₇O₃-m. If the nos. 3–5–9 angle of the former were somehow decreased, the structure would resemble

the latter, and presumably one of the B–O-stretching frequencies could be observed to shift from the 1930–1950 cm⁻¹ range to the upper 1800 cm⁻¹ range. Indeed, IR spectroscopy has been used to assign the identities of smaller, matrix-isolated B_xO_y clusters,³⁸ and the current work suggests that it will be useful for larger clusters as well. These IR results, as well as other calculated and experimental findings, will be discussed further in the following section.

IV. Discussion

Comparison of Present Data with Previous Computational Work on Pure B Clusters. The vast majority of previous computational work on the series of B_xO_y clusters has been performed on those where $y = 0$. While the preponderance of boron in calculations is easy to justify, as its five electrons (three valence) scale well with the N³⁺ scaling of common ab initio approaches, the dearth of calculations with other atoms, save hydrogen, is puzzling. Regardless, given the difficulty in synthesizing and characterizing small boron and boron oxide clusters, a careful consideration of a variety of computational approaches should prove exceedingly informative. Such work begins with the boron dimer.

B₂. The boron dimer has been the subject of many studies, and thus the current discussion should not be considered exhaustive. The current work finds a triplet dimer to be the ground state, in accord with previous studies.^{10,28,29,65} The PW91 calculated bond length of 1.615 Å is in better agreement with the experimental value⁶³ of 1.59 Å than previous work, which finds it to be 1.53 Å with MP2/DZ,²⁹ 1.55 Å using MP4/TZ,²⁸ 1.56 Å using B3LYP/TZ,²⁸ and 1.69 Å using HF/DZ.¹⁰ However, the calculated ZPE-corrected FE of -1.83 eV/B (Table 1) is overbound compared to experiment⁶³ (-1.50 eV/B) and previous calculated values: -1.48, -1.43, -1.46, and -1.22 eV/B, respectively; none of these previous studies appear to contain a ZPE correction.

B₃. The current work finds an equilateral triangle arrangement for B₃ as the global minimum despite the lack of any symmetry constraints, possessing a doublet ground state, a B–B distance of 1.553 Å, and an FE of -3.29 eV/B. This structure is supported by experimental rotational spectroscopy, which finds a *D*_{3h} structure and a bond length of 1.60377 Å.³³ In addition, as before the multiplicity and bond distance calculated herein are in line with previous calculations, which agree on the spin and find distances ranging from 1.52 Å with MP4/TZ²⁸ to 1.582 Å with CCSD(T)/TZ.¹⁶ However, as with the boron dimer,

TABLE 3: Calculated Formation Energies, Lowest Spin State, and Vibrational Frequencies of the Boron Dioxides

cluster ^a	FE (eV/B)	spin ^b	vibrational frequencies (cm ⁻¹)
B ₂ O ₂	-6.80	S	2066, 1899, 606, 492, 425, 228
B ₃ O ₂	-3.51	D	1914, 1904, 1132, 478, 463, 427, 346, 276, 133
B ₄ O ₂	-2.49	T	1991, 1975, 1483, 850, 464, 463, 414, 413, 399, 224, 222, 104
B ₅ O ₂ -d	-1.91	D	1929, 1361, 1315, 1025, 839, 733, 699, 571, 461, 438, 393, 367, 259, 105, 95
B ₅ O ₂ -e	-1.86	D	1724, 1459, 1184, 1098, 965, 798, 771, 622, 492, 462, 420, 382, 289, 178, 124
B ₆ O ₂	-1.79	S	1963, 1485, 1323, 1192, 1005, 942, 816, 772, 591, 520, 515, 483, 420, 396, 351, 234, 95, 76
B ₇ O ₂	-1.34	D	1456, 1373, 1220, 1198, 1107, 1032, 988, 877, 776, 708, 629, 601, 565, 558, 539, 439, 422, 400, 358, 178, 153
B ₈ O ₂	-1.16	S	1632, 1625, 1422, 1407, 1265, 916, 841, 794, 740, 699, 661, 572, 542, 505, 490, 432, 422, 401, 400, 356, 305, 294, 219, 129

^a When a letter follows a cluster, refer to Figure 3 for the identity of each isomer. ^bS = singlet, D = doublet, T = triplet.



Figure 4. Three motifs for oxygen placement with respect to the central boron framework. Gray spheres are boron atoms, black spheres are oxygen atoms. Refer to text for details.

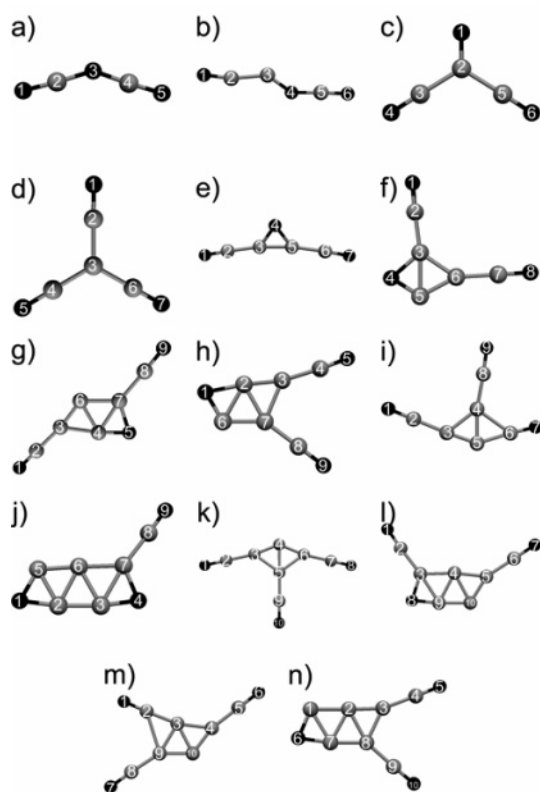


Figure 5. Calculated lowest energy structures of (a) B₂O₃, (b) and (c) B₃O₃, (d) and (e) B₄O₃, (f) B₅O₃, (g), (h), (i), and (j) B₆O₃, (k), (l), (m), and (n) B₇O₃. Gray spheres are boron, black spheres are oxygen. The atom numbers refer to the bond distances given as Supporting Information.

B₃ is again found to be somewhat overbound compared to previous calculations, which finds FEs ranging from -2.01 eV/B with CI/DZ¹⁰ to -3.15 eV/B with B3LYP/TZ.²⁸ Vibrational frequencies were also previously evaluated with B3LYP/TZ,¹⁶ with results (1223 cm⁻¹ and a degenerate vibration at 934 cm⁻¹) clearly in agreement with those given in Table 1. Thus, as with the boron dimer, there seems to be no significant disagreement across a variety of computational methods for the structure and properties of B₃.

B₄. Two low-lying isomers of B₄ were located using the current procedure: the rhombus of Figure 1c and the square of Figure 1d. However, vibrational analysis (Table 1) suggests that only the rhombus is a true minimum with a bond length of

1.533 Å and an FE of -4.00 eV/B. Both Zhai,¹⁶ using B3LYP/TZ and CCSD(T)/TZ, and Boustani,¹⁰ using HF/DZ, found a similar relationship between the two isomers. The former work did not report FEs but rather relative energies with respect to the minimum for a given isomer. Thus, the rhombus and the square differed in their relative FEs by less than 0.01 eV/B, in agreement with the difference of 0.02 eV/B listed in Table 1. The latter work did report FEs, using CI/DZ, and found a separation between the two isomers of 0.02 eV/B in perfect agreement with the current work, although the absolute FE for the rhombus is less than the PW91 result by almost 2 eV/B. Both B3LYP (1.523 Å) and HF (1.528 Å) are within 0.01 Å of the current calculated value, whereas CCSD(T) (1.558 Å) is somewhat farther off but still in agreement.

Other researchers also reported the rhombus geometry but not the square. Bond distances included 1.51 Å with both MP4/TZ and B3LYP/TZ,²⁸ 1.523 Å with B3LYP/TZ,²³ 1.543 Å with QCISD/TZ,²³ and 1.556 Å with MP2/TZ,²⁹ all close to the PW91 value. All rhombi were found to have a singlet spin again in agreement with this work. Jin et al. found,²³ using MP2/TZ, that the linear arrangement was the most stable, favored by 0.28 eV/B over the rhombus. However, given that other MP2/TZ results²⁹ did not reach this conclusion and, indeed, that they were the only computational results not to favor a rhombus, this result is likely in error. Only three FEs have been reported previously: -3.49 eV/B with MP2/TZ,²⁹ -3.62 eV/B with MP4/TZ,²⁸ and -3.79 eV/B with B3LYP/TZ.²⁸ Thus, as before, it seems the PW91 methodology of the current work overestimates stabilities with respect to other computational methods by a few tenths of an eV/B. Finally, vibrational frequencies have been calculated previously,¹⁶ using both B3LYP and CCSD(T) and a TZ basis set. The full set of previous numbers are not duplicated here; the root mean square (rms) difference between PW91 and B3LYP calculated frequencies is 37 cm⁻¹, between PW91 and CCSD(T) is 58 cm⁻¹, and between B3LYP and CCSD(T) is 68 cm⁻¹. Lacking experimental data, it is not possible to say which approach is most accurate in this case.

B₅. At first glance, there is considerable disagreement among previous results for B₅ clusters. For example, both MP4²⁸ and MP2,²⁹ each with a TZ basis, report a trigonal bipyramid minimum energy structure at clear odds with the planar, distorted pentagon shown in Figure 1e. Moreover, the former researchers report that a D_{5h} pentagon is identified as the minimum energy structure with B3LYP, and the latter group reports that HF yields the same result. In each case, the FE is considerably higher than the PW91 value of -4.21 eV/B: -3.63 , -3.51 , -3.67 , and -2.31 eV/B, respectively. However, the tendency of PW91 to overbind has already been noted above even in cases where there was consensus among various methods, and so this discrepancy in and of itself proves little. Additionally, neither group performed a vibrational analysis, to evaluate whether the structures are transition states, saddle points, or minima.

TABLE 4: Calculated Formation Energies, Lowest Spin State, and Vibrational Frequencies of the Boron Trioxides

cluster ^a	FE (eV/B)	spin ^b	vibrational frequencies (cm ⁻¹)
B ₂ O ₃	-8.66	S	2055, 2047, 1228, 718, 508, 475, 457, 451, 105
B ₃ O ₃ -b	-4.81	D	2027, 1897, 1483, 952, 575, 483, 463, 388, 266, 201, 110, 100
B ₃ O ₃ -c	-4.69	D	1967, 1940, 1549, 723, 493, 480, 395, 312, 231, 99, 81, 70
B ₄ O ₃ -d	-3.78	S	1975, 1946, 1923, 932, 929, 569, 473, 452, 426, 301, 267, 243, 98, 80, 56
B ₄ O ₃ -e	-3.73	S	1962, 1951, 1474, 1052, 1075, 654, 549, 497, 444, 410, 340, 211, 196, 132, 113
B ₅ O ₃	-2.90	D	1965, 1957, 1425, 1248, 1086, 709, 669, 518, 499, 481, 435, 412, 374, 336, 152, 130, 115, 53
B ₆ O ₃ -g	-2.42	S	2004, 1989, 1426, 1387, 1118, 951, 715, 673, 604, 539, 481, 474, 450, 392, 376, 348, 271, 192, 117, 75, 69
B ₆ O ₃ -h	-2.42	S	1980, 1971, 1559, 1312, 1175, 944, 829, 735, 522, 486, 471, 442, 411, 406, 368, 347, 233, 137, 121, 103, 53
B ₆ O ₃ -i	-2.42	S	1949, 1937, 1841, 1467, 1209, 808, 639, 584, 470, 458, 450, 396, 386, 333, 317, 194, 180, 165, 123, 113, 83
B ₆ O ₃ -j	-2.41	S	1954, 1515, 1324, 1229, 1028, 1007, 919, 799, 763, 601, 556, 507, 494, 475, 402, 344, 313, 221, 179, 118, 107
B ₇ O ₃ -k	-1.94	D	1958, 1941, 1936, 1411, 1246, 1116, 803, 639, 612, 494, 470, 464, 441, 429, 367, 347, 330, 218, 163, 144, 123, 72, 61, 46
B ₇ O ₃ -l	-1.92	D	1999, 1984, 1469, 1326, 1084, 1020, 846, 834, 767, 606, 562, 515, 484, 463, 418, 403, 403, 343, 258, 231, 117, 110, 71, 64
B ₇ O ₃ -m	-1.92	D	1965, 1962, 1870, 1387, 1216, 1135, 824, 706, 585, 510, 487, 467, 438, 416, 366, 351, 251, 248, 164, 144, 118, 74, 41, 32
B ₇ O ₃ -n	-1.91	D	1941, 1892, 1421, 1369, 1133, 977, 926, 798, 733, 675, 516, 502, 469, 447, 431, 408, 387, 319, 278, 198, 125, 120, 106, 95

^a When a letter follows a cluster, refer to Figure 5 for the identity of each isomer. ^bS = singlet, D = doublet.

To further complicate matters, additional calculations²⁴ with B3LYP/TZ and MP2/TZ both identify the structure in Figure 1e as the global minimum, possessing all real frequencies, a doublet ground state, and with an rms difference for bond distances of 0.006 and 0.013 Å, respectively, from the PW91 structure. Other work¹⁷ using B3LYP, CASSCF, and CCSD(T), all with a TZ basis, also locate this structure with deviations from the PW91 structure of 0.006, 0.015, and 0.025 Å, respectively. The most likely explanation is that symmetry restrictions prevented the workers in refs 28 and 29 from locating the unintuitive, distorted pentagon. We deem this structure to most likely be the global minimum, as not only was it identified by the MD procedure of this paper, but also as it is explicitly calculated in both refs 17 and 24 to be more stable than the trigonal bipyramid; the *D*_{5h} pentagon is not noted as a stationary point in either of these latter two studies. Unfortunately, neither reference reports FEs to compare with the present work. Frequencies were reported¹⁷ at both the B3LYP and CASSCF levels with rms differences of 31 and 58 cm⁻¹, respectively, compared to PW91, and of 33 cm⁻¹ compared to each other.

*B*₆. The pentagonal pyramidal structure of Figure 1f is identified, to the best of our knowledge, as a low energy, but not always minimum energy, structure in every computational study. Niu et al.²⁸ and Park et al.²⁹ both identify it as the lowest energy orientation of B₆ with FEs of -4.23 eV/B at the B3LYP/TZ level,²⁸ -3.64 eV/B at the MP4/TZ level,²⁸ and -3.80 eV/B at the MP2/TZ level.²⁹ The PW91 calculated FE of -4.45 eV/B clearly agrees most with the other DFT result. Neither group considered the structure shown in Figure 1g.

Both B₆ structures in Figure 1 were considered by Li et al.²⁵ with a singlet *C*_{5v} structure as the minimum energy structure using HF, B3LYP, B3PW91, and MP2, each paired with a TZ basis. Additionally, vibrational analysis confirmed the finding in Table 1 of no imaginary frequencies. For each of these techniques, save HF, the next most stable isomer, also without any imaginary frequencies, is the one shown in Figure 1g, although Li and co-workers assign it a singlet ground state, as compared to the triplet ground state found in this work. Formation energies are given relative to the *C*_{5v} isomer and are +0.16, 0.20, and 0.20 eV/B for B3LYP, B3PW91, and MP2, respectively. In contrast, PW91 finds a gap (Table 1) of only 0.01 eV/B in the FEs of the two isomers of B₆. Other computational results are in closer agreement with PW91. For example, Guerini et al.,³² using CCSD(T) and a DZ basis, found that the structure in Figure 1f possesses no imaginary frequencies

and is more stable than the structure of Figure 1g by 0.03 eV/B; vibrational results are not given for the latter isomer. Ma et al.³¹ found, using B3LYP/TZ, a separation of 0.01 eV/B between the two isomers, as in the present study, the same spins as in this work and no imaginary frequencies for either isomer but with a reversed order of stability with respect to the PW91 results. The results of Alexandrova and co-workers,¹⁸ also using B3LYP/TZ, agreed with Ma et al. but found that CCSD(T)/TZ gave the same ordering as PW91 with a difference in FEs of 0.05 eV/B. Thus, while there does not seem to be agreement across methods on which isomer is lower in energy, there does seem to be a strong indication that both hexamers are likely to be experimentally relevant. On a final note, the frequencies of the structure in Figure 1f are calculated elsewhere^{18,32} with B3LYP and different basis sets; the rms difference of the frequencies with respect to the PW91 calculated values are 12 and 8 cm⁻¹, respectively, for refs 18 and 32. This agreement is tremendous, especially considering that the two sets of B3LYP data have an rms difference of 8 cm⁻¹ with respect to each other, indicating a basis set effect on par with the effect of the choice of functional.

*B*₇. In contrast to B₆, there is considerable consensus about the structure of B₇, which overwhelmingly favors that shown in Figure 1h. B3LYP,^{19,26} B3PW91,²⁶ and MP2²⁶ all find this structure, in a doublet spin state and with all real frequencies, far more stable than any other heptamer arrangement, as do HF¹⁰ and an uncommon linear-muffin-tin-orbital approach.³⁰ The FEs given by these last two methods, -3.06 and -5.24 eV/B, respectively, bracket the calculated PW91 value of -4.71 eV/B. The rms difference between the PW91 frequencies and those calculated with B3LYP/TZ¹⁹ is 19 cm⁻¹, further indicating that these two approaches agree closely on the identity of this isomer.

*B*₈. The literature is also in agreement about the structure of B₈, depicted in Figure 1i. Zhai et al.²⁰ used a combination of photoelectron spectroscopy and B3LYP calculations, both of which indicated a *D*_{7h} structure and a triplet ground state, in agreement with this work. Boustani¹⁰ had already predicted this structure and spin using HF with a CI-corrected FE of -3.34 eV/B. This differs greatly from the -4.98 eV/B calculated with PW91, as have all of the CI values. Li et al.²⁷ used B3LYP, B3PW91, and MP2/TZ, all of which recommend this planar, triplet structure. No imaginary frequencies were found for this structure with any of these approaches, and the rms differences compared to the PW91 frequencies are 12, 8, and 57 cm⁻¹, respectively.

B₉. Few results have been reported for B₉ in the past decade. Boustani's HF/DZ results¹⁰ indicate two low-lying isomers: a *D*_{7h} isomer, as shown in Figure 1j, and a *C*_s isomer, which can be envisioned as this *D*_{7h} isomer stretched along an axis perpendicular to the axis of the central pair of boron atoms. A difference of 0.03 eV/B in the FEs of these two species is also given. In contrast, a combined experimental/computational report²⁰ finds a nearly *D*_{8h} arrangement with only a single central boron. It is unclear how many isomers were computed, although given that reference was made to Boustani's work,¹⁰ it seems reasonable to assume that the structure in Figure 1j was indeed considered. Unfortunately, it is also unclear if the accuracy of the experimental photoelectron spectrum was sufficient to distinguish between the two centrosymmetric isomers of *D*_{7h} and *D*_{8h} symmetry. Complicating matters is the fact that the experimental work dealt with B₉⁻, as opposed to the neutral species of interest in this work. However, other computational studies^{22–26} have found that boron cluster geometries tend to change little upon introduction of a charge, and thus it is theoretically possible that further work will permit the establishment of qualitative connections between experiment and theory. In any case, more work is required before a ground state of B₉ can be definitively determined.

B₁₀. As with B₉, few studies have considered the boron decamer. Boustani¹⁰ again reported, using HF/DZ, a structure in accord with the present PW91 results (Figure 1k) with a calculated FE of -3.41 eV/B (cf. -5.17 eV/B in this study). He also found a second, structurally similar isomer that was calculated to be only 0.05 eV/B less stable. Using a linear-muffin-tin-orbital approach, however, Cao et al.³⁰ found that this second isomer collapsed to the structure shown in Figure 1k upon geometry optimization, a finding supported by the current results. The calculated FE of -5.78 eV/B is overbound compared to the PW91 calculated value, as was the case with B₇.

Summary of Pure Boron Work. There appears to be a significant amount of consensus for most of the boron species. Unambiguous identities, at least based upon the computational work cited here, can be offered for the structures of B₂–B₄ as well as B₇ and B₈; Figure 1 depicts these structures with the note that Figure 1d is almost certainly a transition state. In addition, if one entertains the possibility that symmetry constrains hampered early work,^{28,29} Figure 1e can be taken as the consensus structure for B₅. There is, simply stated, no consensus as to which isomer of B₆ is the global minimum, although there is agreement that both isomers are stable and very close in energy. The lack of consensus about the structure of B₉ is more likely a reflection of a lack of data, rather than any fundamental computational disagreement. Finally, for B₁₀ the little data in the literature do all agree upon the structure shown in Figure 1k. On a final structural note, the need to explore a wealth of structures, either through an energy-based sampling method as in this work or through an extensive variety of initial geometries, is clearly necessary to find agreement about structural assignment. In other words, computational disagreement for these clusters may often simply be no more than sampling error. This point is especially critical as non-boron atoms are incorporated, leading to much greater potential structural variability.

Observations can also be made about the three quantities often evaluated for these clusters: geometry parameters, (relative) stabilities, and vibrational frequencies. Calculated bond distances seem to be fairly straightforward to obtain accurately, as various methods tend to give predictions within a few hundredths of

an angstrom of each other, certainly an acceptable level of precision. Discouragingly, there seems to be no such accuracy in evaluating cluster energetics. However, as will be discussed later, there are indications that reliable trends are observed, at least with PW91, even if absolute accuracy proves elusive. Boustani's values,¹⁰ in stark absolute disagreement with the current calculated values, also produce the same, experimentally verified trend (see below). In regard to calculated frequencies with few exceptions, all techniques seem to perform well in distinguishing true minima from saddle points. In addition, different methods seem to deviate from each other on the order of tens of wavenumbers and often less, which seems to indicate that a combination of experimental and computational measurement of vibrational frequencies should prove a powerful structural probe. This expectation is also borne out in small boron oxide clusters, which will now be considered.

Previous Work on Boron Oxide Clusters. In contrast to pure boron clusters, only a limited amount of research has been done on isolated boron oxide clusters; work has also been performed on the bulk crystalline B₂O₃ polymorphs (see refs 58, 59, and references therein) and the common glassy B₂O₃ form (see refs 53, 54, and references therein). Nevertheless, some results have been given for isolated clusters of small boron oxides. Photoelectron spectroscopy paired with HF/DZ and MP3/DZ calculations³⁵ concluded that B₂O₂ possesses the structure shown in Figure 3a; other possible arrangements, such as linear BOOB or any bent configurations, were found to be less stable by at least 0.73 eV. Bond distances for the O–B and B–B distances were calculated, respectively, as 1.182 and 1.668 Å with HF and 1.201 and 1.647 Å with MP3 in generally close agreement with the PW91 values of 1.207 and 1.631 Å, respectively. Moreover, vibrational frequencies were reported with each technique with the rms difference from the PW91 results being 109 and 93 cm⁻¹, respectively. However, the PW91 results are much closer to the experimental data⁶⁶ (rms difference = 36 cm⁻¹) than are HF and MP3 with respective deviations of 126 and 94 cm⁻¹. Thus, based on these B₂O₂ results, the PW91 approach in this paper seems to be very useful in evaluating vibrational spectra of boron oxides.

Another diboron oxide, B₂O₃, has been evaluated using a B3LYP/TZ methodology.⁴⁰ The reported structure is nearly identical to that shown in Figure 5a with distances agreeing to 0.01 Å and bond angles to 2.2°. Their vibrational analysis found no imaginary frequencies in agreement with the results in Table 4. B3LYP also identified the linear isomer as being within 0.01 eV/B of the bent shape shown in Figure 5a, although this structure was not found with either the present approach or identified as a minimum with MP2/DZ.³⁹ A final piece of information is the experimental measurement³⁸ of 2062 cm⁻¹ for the most naturally abundant ¹¹B¹⁶O isotopomer in clear agreement with the asymmetric stretch calculated with PW91 of 2067 cm⁻¹. Thus, despite possible indications of a second low-energy isomer, it seems likely that the structure in Figure 5a is an accurate depiction of isolated B₂O₃. It should also be noted that neither MP2/DZ nor HF/DZ were accurate in predicting the asymmetric stretch of B₂O₃ with errors of 63 and 221 cm⁻¹, respectively,³⁹ again suggesting that PW91 provides superior vibrational frequencies.

Finally, MP2 was also used in ref 39 to investigate three other boron oxide species not yet mentioned. Doublet boron monoxide was found to have a bond distance of 1.216 Å and a stretching frequency of 1936 cm⁻¹, as compared to 1.216 Å and 1869 cm⁻¹ with PW91; the current work is again more accurate when compared to the experimentally measured⁶³ stretching

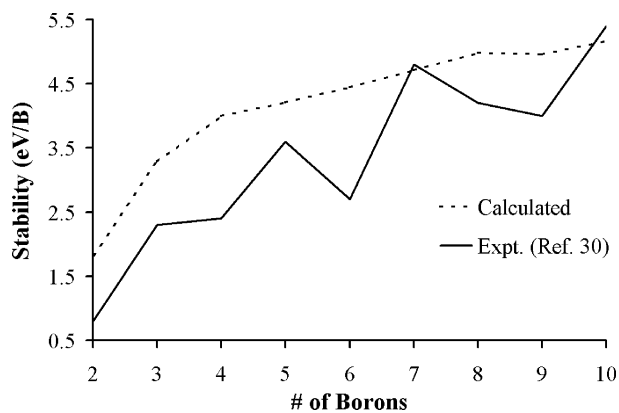


Figure 6. Comparison of the experimental lowest energy fragmentation appearance potential (solid line) with the PW91-calculated formation energies of this work (dashed line).

frequency of 1886 cm^{-1} . MP2 was also used to calculate B_2O , indicating a nearly linear BOB arrangement, as given in Figure 2b, with a B–O bond length of 1.329 \AA and vibrational frequencies of 1456 , 1043 , and 24 cm^{-1} . The PW91 results show a nearly identical bond length of 1.327 \AA and calculated frequencies of 1480 , 1053 , and 111 cm^{-1} . The experimental frequencies³⁸ are 1447 , 1052 , and 107 cm^{-1} , which is sufficient accuracy to not only confirm the structure in Figure 2b as the minimum energy structure of B_2O , but also to further indicate the accuracy of PW91-calculated frequencies. Finally, Nemukhin et al.³⁹ proposed an isomer of B_3O_3 consisting of a hexagonal ring with alternating boron and oxygen atoms. This structure clearly differs from those shown in Figure 5b,c, and thus further work is necessary before a minimum energy structure can definitively be assigned.

To summarize, the few computational and experimental results seem to be in agreement about the identities of BO , B_2O_2 , and B_2O_3 , depicted in Figures 2a, 3a, and 5a, respectively. However, PW91 seems to deliver vibrational frequencies far superior to other computational methods, as measured by comparison to both gas phase⁶³ and frozen matrix^{38,66} experimental data. Thus, as further experiments on boron oxides are performed, the frequencies in Tables 2, 3, and 4 should provide a useful guide in determining boron oxide structure.

Evaluation of Collision-Induced Dissociation Data in the Context of the Present Work. One body of work that has not yet been addressed is the collision-induced dissociation (CID) data of Anderson and co-workers. In this series of papers, laser-ablated boron clusters were mass selected and then were collided with Xe ,³⁴ O_2 ,³⁶ and CO_2 .³⁷ The resulting dissociation energies and ionization potentials were used to infer cluster stabilities and even some structural data, both of which should be comparable to the results of this paper. The largest difficulty in comparing this work with these experiments is that, as the latter rely on mass spectrometry, the clusters analyzed all carry a positive charge, whereas only neutral clusters are evaluated in this work. However, as noted above, charge does not greatly influence boron cluster geometries, and thus, as will be seen, qualitative connections between experiment and theory can be established.

The most significant finding of the collision of cationic boron clusters with xenon³⁴ is that cluster stabilities increase with increasing cluster size, albeit with some exceptions. Figure 6 compares the lowest experimental cluster appearance potentials with the magnitude of the FEs listed in Table 1. As noted earlier, while the quantitative agreement is rather poor, even considering the fairly large (about 0.6 eV) experimental error bars, the

general upward trend is reproduced by the calculations. However, while the experiment shows a decrease in stability from the pentamer to the hexamer, from the heptamer to the octamer, and from the octamer to the nonamer, only the latter decrease is found in the calculated results. Further work using the methodology of this paper that explicitly considers the positive charge may explain these deviations from experiment. Even without such data, the current study does not support the conjecture³⁴ that increased stability as a function of cluster size is due to a greater tendency toward 3D structures. As Figure 1 suggests, this trend is instead attributable to increasingly extensive two-dimensional arrangements with increasing cluster size.

A number of findings in the O_2 CID work³⁶ can also be correlated to results of the current study. Although it was noted that collision with oxygen is too energetic to routinely produce stable boron oxides, save BO^+ and B_2O^+ , information about the structures of the pure boron clusters was ascertained. For example, it was conjectured that two isomers of B_4^+ and B_6^+ may exist, which is certainly in line with the findings of this study (see Figure 1 and Table 1). Furthermore, this experimental finding suggests that $\text{B}_4\text{-d}$ may be a long-lived metastable transition state, if not a genuine minimum altogether. In addition, B_9^+ was singled out as being particularly unstable, which fits with its role as the only cluster computed to be less stable on a per boron basis than its B_{x-1} analogue (Figure 6). Finally, the authors noted with some surprise that for B_7^+ and all larger clusters the binding energy per oxygen atom decreases with increasing boron cluster size. For example, the oxygen in B_8O^+ is less tightly bound to the boron core than is the oxygen in B_7O^+ . As can be seen from Tables 2, 3, and 4, and as will be discussed in more detail shortly, the present calculations suggest that this trend is true for any boron cluster and not simply for those larger than B_7 .

The final CID study³⁷ utilized CO_2 as an oxygen source, which produced gentler collisions and therefore greater insight into boron oxide structures, as well as additional information about pure boron clusters. On the basis of the data, it was postulated that B_6O^+ , B_8O^+ , and B_9O^+ possess a central “core” with a B–O moiety extending outward. $\text{B}_6\text{O-i}$ and $\text{B}_9\text{O-l}$ (Figure 2) fit with this pattern, but the calculated minimum energy structure of B_8O does not possess this arrangement. Another experimental observation about the monoxides is that B_5O^+ is particularly stable. A possible reflection of this finding is seen in Table 2 where the FE of $\text{B}_5\text{O-g}$ (-0.96 eV/B) is lower than both its lighter neighbor ($\text{B}_4\text{O-d}$, -0.87 eV/B) and its heavier neighbor (B_6O , -0.91 eV/B). No other monoxide has this characteristic. Despite the good agreement on these two findings, the experimental research also suggests the possible existence of two isomers of B_8O^+ , which is not found in the present work. Similarly, it was postulated that B_8^+ may have two low-lying isomers, also in disagreement with the PW91 results.

The most significant finding of the CO_2 CID work is confirmation that oxygen is bound less tightly to larger clusters. Indeed, whereas the O_2 CID indicated that this might be true for clusters of $7+$ boron atoms, the CO_2 data indicate that this trend may begin as early as the tetramer. To compare this experimental finding with the current work, Figure 7 shows the ZPE-corrected FEs of the monoxides, dioxides, trioxides, and bare boron clusters. The FEs of bulk β -boron and bulk B_2O_3 , indicated by horizontal dashed and solid lines, respectively, are not ZPE-corrected. Figure 7 also includes results for three highly oxidized species, B_5O_5 , B_3O_6 , and B_4O_6 , which because of their

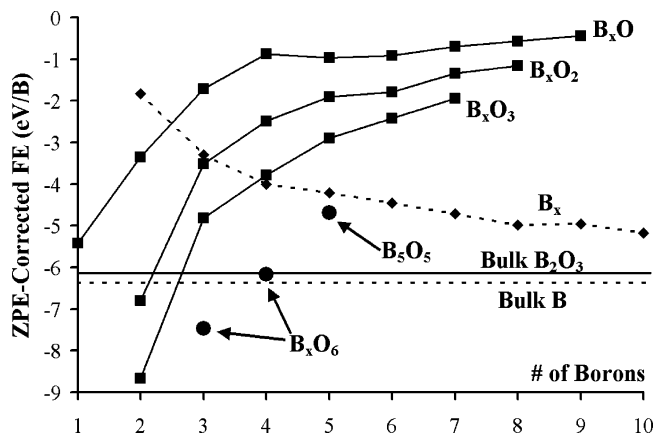


Figure 7. PW91-calculated, zero-point energy corrected formation energies in eV per boron for the most stable isomers of the clusters in this study. Solid lines correspond to the cluster and bulk oxides as labeled; dashed lines are for the boron clusters and bulk β -boron. Preliminary results for pentoxide and hexoxide clusters are also shown as labeled circles.

preliminary nature⁶⁷ should be taken as the upper limit of the FEs for these species. Clearly, given that nearly all B_xO_y clusters are less stable than their $B_{x-1}O_y$ counterparts, PW91 indicates a finding in line with the CO_2 CID data, which predict an early onset of such a phenomenon. In fact, Anderson et al. suggest that B_2^+ and B_3^+ should be much more reactive, and therefore the corresponding monoxides much more stable, than they are found to be experimentally. However, because of their small size, they perhaps cannot adequately stabilize the intermediate $B_2^+-CO_2$ and $B_3^+-CO_2$ complexes necessary to form monoxides. If this supposition is considered true, then the experimental findings are truly in line with the PW91 results, where the trend of decreasing B–O energy with increasing cluster size extends all the way down to the boron dimer.

This trend in decreasing B–O energy puts upper limits on the range of oxidizability. For example, it was noted experimentally³⁷ that $B_{12}O^+$ does not form from B_{12}^+ . Such a finding could be consistent with the computational result; a linear extrapolation of the FEs of B_7O , B_8O , and B_9O suggests that $B_{12}O$ would have a FE close to zero eV/B. Although there is no particular reason to favor a linear extrapolation over, for example, an asymptotic approach to 0, the result is nonetheless reassuring, especially given the earlier noted concerns about the accuracy of calculated FEs. The lower oxidizability of larger boron clusters was also observed experimentally for higher-order oxides, as B_6^+ was observed to produce up to a hexoxide cluster as the pressure of CO_2 was increased, but B_9^+ could only form a trioxide. However, given the computational results in Figure 7, it is difficult to see how, for example, B_9O_3 would represent an upper limit to boron nonamer oxidation, given that B_9O is stable and that each higher-order oxide curve is lower in FE than its lower-order neighbor. Moreover, based on the two hexoxide data points, it seems likely that higher-order oxide curves are shaped similarly to the full curves shown in Figure 7, simply shifted to increased stabilities. Thus, it appears that further experimental and computational work is needed before the limits of boron oxidizability can be firmly established.

We conclude our discussion with some observations about the transition from cluster behavior to bulk behavior. For the bare boron clusters, B_{10} is 1.2 eV/B less stable than the bulk arrangement. Moreover, the quasiplanar structure of this cluster differs vastly from the bulk structure, which is characterized by intricate 3D arrangements of B_{12} icosahedra.³ Clearly, the current work offers scant insight into the transition point from

cluster to bulk, except to state that it definitely has not occurred at the decamer. With regards to the transition from small boron oxide clusters to bulk B_2O_3 , answers are similarly lacking, notwithstanding the serendipitous finding that the FE of isolated B_4O_6 , -6.17 eV/B, is nearly identical to the FE of bulk B_2O_3 , -6.14 eV/B. The best hypothesis at this point is that higher-order oxide curves will continue to be shifted to greater stabilities, as, for example, the trioxide curve is lower in energy than the monoxide curve, and as the preliminary hexoxide curve is shifted further still to lower energies. As the curves shift lower, the asymptote with respect to cluster size will eventually collapse to the horizontal bulk B_2O_3 line shown in Figure 7. As with the pure boron clusters, the most definitive answer provided by this study is that the transition to bulk behavior has not yet occurred at 10 atoms.

V. Conclusion

DFT calculations using the PW91 functional in conjunction with a plane-wave basis set and a pseudopotential were employed to investigate the structure, vibrational characteristics, and energetics of small (up to 10 atom) boron and boron oxide clusters. The problem of locating the global minimum for each species on its potential energy surface was addressed through extensive quantum molecular dynamics sampling, starting from a variety of possible geometries. The resulting structures tend to be planar, and many of the same structural motifs first elucidated in the pure boron clusters are observed in the oxide species. Oxygen generally adds to the exterior of the boron cluster with individual oxygen atoms spaced apart from one another and can be found either attached to a single boron atom or bridging across a pair of boron atoms. Careful consideration of the calculated vibrational frequencies reveals that a further subdivision can be made for oxygen atoms bound to a single boron atom, as this boron can in turn be attached to either a single boron or to a pair of boron atoms. The three possible orientations possess B–O-stretching frequencies at different energies, similar to the bridging and terminal-stretching frequency regions of C–O, and thus can be distinguished on the basis of vibrational spectroscopy. Evidence indicates that oxygen prefers to occupy the bridging position, but with multiple oxygen atoms, satisfying this condition requires a fairly extensive structure. As a result, most small di- and trioxide clusters possess both terminal and bridging oxygen atoms.

Comparison with previous computational studies revealed a great deal of consensus about the most stable structures for B_2 , B_3 , B_4 , B_7 , and B_8 . An oversight in previous calculations is suggested that leads to a similar degree of accord about the structure of B_5 as well. Additionally, most previous studies, as well as the current work, agree about the existence of two stable B_6 isomers, although there is decidedly no consensus about which is the most stable. Further computational research is needed to conclusively determine the minimum energy structures of B_9 and B_{10} , although it should be noted that the existing body of work does agree on the structure of the latter, but not the former.

Bond distances seem to be fairly consistent regardless of the computational methodology used and are quite reasonable compared to the few available experimentally measured values. There is less consensus in the calculation of vibrational frequencies, although comparison with experimental results of boron oxides suggests that PW91 is more accurate than both hybrid DFT calculations, such as B3LYP, and wavefunction based approaches, such as HF and MP2. It is therefore our expectation that future experimental studies using IR spectros-

copy can benefit greatly from the calculated frequencies given in this paper, which can perhaps act as fingerprints for the structures reported here.

Calculated formation energies, when reported elsewhere in the literature, vary widely from each other and from the results of this work. Furthermore, bulk calculations with PW91 suggest that errors on the order of 0.5 eV/B are to be expected with this approach. However, meaningful results can still be obtained, as revealed through comparison with experimental mass spectrometry data. The experimental trend of increasing boron cluster stability with increasing cluster size is found using PW91, as is the trend of decreasing stability with increasing cluster size for the boron oxides. Because of this latter trend, it is experimentally found that B₁₂O is the largest monoxide cluster that can form, a finding that is consistent with the computational work reported herein. Additionally, many of the structural inferences made based on experimentally measured cluster stabilities are either confirmed or clarified. However, it was also found, based on both structural and energetic information, that the transition between cluster behavior and bulk behavior is certainly not attained under the 10 atom limit applied in this study.

The most obvious extension of this work is to increase the sizes of the clusters studied. Many conjectures offered in this current work can be readily judged by evaluating larger structures, such as the preference of oxygen for bridging sites or the lack of stability for B₁₃O. Moreover, increasing the number of oxygen atoms in the clusters, as has been done preliminarily for B₅O₅, B₃O₆, and B₄O₆, should enable further insight into the transition from isolated boron oxide clusters to bulk B₂O₃. It appears, however, that both this transition, as well as the change from cluster to bulk for pure boron, is at a fairly large size. Therefore, a more fruitful line of research may be the investigation, using quantum molecular dynamics, of the addition of oxygen to large, bulklike boron fragments. Additionally, it may prove informative to computationally model the exposure of a crystal plane of bulk boron to gaseous oxygen molecules. In any event, the results provided in this paper provide a fundamental basis for developing an understanding of boron oxidation at a molecular level and will be required for new applications such as the engineering of a nanoscale, high-energy fuel source.

Acknowledgment. Research was sponsored by the Laboratory Directed Research and Development Program of Oak Ridge National Laboratory and by the Division of Materials Science, U.S. Department of Energy under Contract No. DEAC05-00OR22725 with UT-Battelle, LLC at Oak Ridge National Laboratory. The extensive computations were performed using the resources of the National Center for Computational Sciences at ORNL.

Supporting Information Available: Bond distances for each of the isomers shown in Figures 1–3, 5 of this paper. This material is available free of charge via the Internet at <http://pubs.acs.org>.

References and Notes

- (1) (a) *Boron, Metallo-Boron Compounds, and Boranes*; Adams, R. M., Ed.; Interscience Publishers: New York, 1964. (b) *Boron and Refractory Borides*; Matkovich, V. I., Ed.; Springer-Verlag: Berlin, 1977. (c) Hoard, J. L.; Sullenger, D. B.; Kennard, C. H. L.; Hughes, R. E. *J. Solid State Chem.* **1970**, *1*, 268.
- (2) Geist, D.; Kloss, R.; Follner, H. *Acta Crystallogr., Sect B* **1970**, *26*, 1800.
- (3) Donohue, J. *The Structures of the Elements*; John Wiley & Sons: New York, 1974.
- (4) Plešek, J. *Chem. Rev.* **1992**, *92*, 269.
- (5) Slattery, D. K.; Hampton, M. D. *Proceedings of the 2002 US DOE Hydrogen Program Review*, NREL/CP-610–32405.
- (6) Meinköhn, D. *Combust. Flame* **1985**, *59*, 225.
- (7) King, M. K. *J. Spacecr. Rockets* **1982**, *19*, 294.
- (8) Faeth, G. M. *Prog. Energy Combust. Sci.* **1983**, *9*, 1.
- (9) Boustani, I. *Chem. Phys. Lett.* **1995**, *240*, 135.
- (10) Boustani, I. *Phys. Rev. B* **1997**, *55*, 16426.
- (11) Kato, H.; Tanaka, E. *J. Comput. Chem.* **1991**, *12*, 1097.
- (12) Ray, A. K.; Howard, I. A.; Kanal, K. M. *Phys. Rev. B* **1992**, *45*, 14247.
- (13) Kato, H.; Yamashita, K. *Chem. Phys. Lett.* **1992**, *190*, 361.
- (14) Chacko, S.; Kanhere, D. G.; Boustani, I. *Phys. Rev. B* **2003**, *68*, 035414.
- (15) Kiran, B.; Bulusu, S.; Zhai, H.-J.; Yoo, S.; Zeng, X. C.; Wang, L.-S. *Proc. Natl. Acad. Sci. U.S.A.* **2005**, *102*, 961.
- (16) Zhai, H. J.; Wang, L. S.; Alexandrova, A. N.; Boldyrev, A. I.; Zakrzewski, V. G. *J. Phys. Chem. A* **2003**, *107*, 9319.
- (17) Zhai, H. J.; Wang, L. S.; Alexandrova, A. N.; Boldyrev, A. I. *J. Chem. Phys.* **2002**, *117*, 7917.
- (18) Alexandrova, A. N.; Boldyrev, A. I.; Zhai, H. J.; Wang, L. S.; Steiner, E.; Fowler, P. W. *J. Phys. Chem. A* **2003**, *107*, 1359.
- (19) Alexandrova, A. N.; Boldyrev, A. I.; Zhai, H. J.; Wang, L. S. *J. Phys. Chem. A* **2004**, *108*, 3509.
- (20) (a) Zhai, H. J.; Alexandrova, A. N.; Birch, K. A.; Boldyrev, A. I.; Wang, L. S. *Angew. Chem., Int. Ed.* **2003**, *42*, 6004. (b) Zhai, H.-J.; Kiran, B.; Li, J.; Wang, L.-S. *Nat. Mater.* **2003**, *2*, 827.
- (21) Zhai, H.-J.; Wang, L.-M.; Li, S.-D.; Wang, L.-S. *J. Phys. Chem. A* **2007**, *111*, 1030.
- (22) Alexandrova, A. N.; Boldyrev, A. I.; Zhai, H.-J.; Wang, L.-S. *Coord. Chem. Rev.* **2006**, *250*, 2811.
- (23) Jin, H. W.; Li, Q. S. *Phys. Chem. Chem. Phys.* **2003**, *5*, 1110.
- (24) Li, Q. S.; Jin, H. W. *J. Phys. Chem. A* **2002**, *106*, 7042.
- (25) Li, Q. S.; Jin, Q.; Luo, Q.; Tang, A. C.; Yu, J. K.; Zhang, H. X. *Int. J. Quantum Chem.* **2003**, *94*, 269.
- (26) Li, Q. S.; Gong, L. F.; Gao, Z. M. *Chem. Phys. Lett.* **2004**, *390*, 220.
- (27) Li, Q.; Zhao, Y.; Xu, W.; Li, N. *Int. J. Quantum Chem.* **2005**, *101*, 219.
- (28) Niu, J.; Rao, B. K.; Jena, P. *J. Chem. Phys.* **1997**, *107*, 132.
- (29) Park, J. H.; Lee, J. I.; Kim, M. K.; Oh, Y. K.; Cho, H. S. *J. Korean Phys. Soc.* **1999**, *34*, 268.
- (30) Cao, P. L.; Zhao, W.; Li, B. X.; Song, B.; Zhou, X. Y. *J. Phys.: Condens. Matter* **2001**, *13*, 5065.
- (31) Ma, J.; Li, Z.; Fan, K.; Zhou, M. *Chem. Phys. Lett.* **2003**, *372*, 708.
- (32) Guerini, S.; Piquini, P. *Int. J. Quantum Chem.* **2003**, *95*, 329.
- (33) Cias, P.; Araki, M.; Denisov, A.; Maier, J. P. *J. Chem. Phys.* **2004**, *121*, 6776.
- (34) Hanley, L.; Whitten, J. L.; Anderson, S. L. *J. Phys. Chem.* **1988**, *92*, 5803.
- (35) Ruščić, B. M.; Curtiss, L. A.; Berkowitz, J. *J. Chem. Phys.* **1984**, *80*, 3962.
- (36) Hanley, L.; Anderson, S. L. *J. Chem. Phys.* **1988**, *89*, 2848.
- (37) Ruatta, S. A.; Hintz, P. A.; Anderson, S. L. *J. Chem. Phys.* **1991**, *94*, 2833.
- (38) Burkholder, T. R.; Andrews, L. *J. Chem. Phys.* **1991**, *95*, 8697.
- (39) Nemukhin, A. V.; Weinhold, F. *J. Chem. Phys.* **1993**, *98*, 1329.
- (40) Jemmis, E. D.; Giju, K. T.; Leszczynski, J. *Electron J. Theor. Chem.* **1997**, *2*, 130.
- (41) Xu, Y.; Shelton, W. A.; Schneider, W. F. *J. Phys. Chem. A* **2006**, *110*, 5839.
- (42) Balasubramanian, K. *Chem. Phys. Lett.* **1988**, *150*, 71.
- (43) (a) Kresse, G.; Hafner, J. *Phys. Rev. B* **1993**, *47*, 558. (b) Kresse, G.; Hafner, J. *Phys. Rev. B* **1994**, *49*, 14251.
- (44) (a) Kresse, G.; Furthmüller, J. *Comput. Mat. Sci.* **1996**, *6*, 15. (b) Kresse, G.; Furthmüller, J. *Phys. Rev. B* **1996**, *54*, 11169.
- (45) Blöchl, P. E. *Phys. Rev. B* **1994**, *50*, 17953.
- (46) Kresse, G.; Joubert, D. *Phys. Rev. B* **1999**, *59*, 1758.
- (47) (a) Perdew, J. P.; Chevary, J. A.; Vosko, S. H.; Jackson, K. A.; Pederson, M. R.; Singh, D. J.; Fiolhais, C. *Phys. Rev. B* **1992**, *46*, 6671. (b) Perdew, J. P.; Chevary, J. A.; Vosko, S. H.; Jackson, K. A.; Pederson, M. R.; Singh, D. J.; Fiolhais, C. *Phys. Rev. B* **1993**, *48*, 4978.
- (48) Monkhorst, H. J.; Pack, J. D. *Phys. Rev. B* **1976**, *13*, 5188.
- (49) Press, W. H.; Flannery, B. P.; Teukolsky, S. A.; Vetterling, W. T. *Numerical Recipes in C: The Art of Scientific Computing*; Cambridge University Press: Cambridge, England, 1988.
- (50) Pulay, P. *Chem. Phys. Lett.* **1980**, *73*, 393.
- (51) Nosé, S. *J. Chem. Phys.* **1984**, *81*, 511.
- (52) High Performance Computational Chemistry Group, "NWChem, A Computational Chemistry Package for Parallel Computers, Version 4.7" (2005), Pacific Northwest National Laboratory, Richland, WA.

- (53) Amini, M.; Mitra, S. K.; Hockney, R. W. *J. Phys. C: Solid State Phys.* **1981**, *14*, 3689.
- (54) Maranas, J. K.; Chen, Y.; Stillinger, D. K.; Stillinger, F. H. *J. Chem. Phys.* **2001**, *115*, 6578.
- (55) Gurr, G. E.; Montgomery, P. W.; Knutson, C. D.; Gorres, B. T. *Acta Crystallogr., Sect. B* **1970**, *26*, 906.
- (56) Effenberger, H.; Lengauer, C. L.; Parthé, E. *Monatsh. Chem.* **2001**, *132*, 1515.
- (57) Nelmes, R. J.; Loveday, J. S.; Allan, D. R.; Besson, J. M.; Hamel, G.; Grima, P.; Hull, S. *Phys. Rev. B* **1993**, *47*, 7668.
- (58) Takada, A.; Catlow, C. R. A.; Lin, J. S.; Price, G. D.; Lee, M. H.; Milman, V.; Payne, M. C. *Phys. Rev. B* **1995**, *51*, 1447.
- (59) Engberg, U. *Phys. Rev. B* **1997**, *55*, 2824.
- (60) Nobes, R. H.; Akhmatkaya, E. V.; Milman, V.; Winkler, B.; Pickard, C. J. *Comput. Mater. Sci.* **2000**, *17*, 141.
- (61) Kittel, C. *Introduction to Solid State Physics*, 7th Edition; Wiley: New York, 1996.
- (62) Chase, M. W., Jr. *J. Phys. Chem. Ref. Data* **1998**, *9*, 1.
- (63) Huber, K. P.; Herzberg, G. *Molecular Spectra and Molecular Structure IV. Constants of Diatomic Molecules*; Van Nostrand: New York, 1979.
- (64) Zubarev, D. Y.; Boldyrev, A. I. *J. Comput. Chem.* **2007**, *28*, 251.
- (65) Bruna, P. J.; Wright, J. S. *J. Phys. Chem.* **1990**, *94*, 1774.
- (66) Serebrennikov, L. V. *Vestn. Mosk. Univ., Ser. 2: Khim.* **1981**, *22*, 606.
- (67) These results are considered preliminary because the high oxygen content tends to lead the clusters in our MD simulations to fragment, thus requiring a procedure that samples fewer distinct geometries, in turn leading to longer MD trajectories and greater uncertainty about the location of the true global minimum.